

# On the Ergodic Capacity for SIM-Aided Holographic MIMO Communications

Anastasios Papazafeiropoulos, Ioannis Bartsikas, Dimitra I. Kaklamani, Iakovos S. Venieris

**Abstract**—We derive a novel closed-form lower bound on the ergodic capacity of holographic multiple-input multiple-output (HMIMO) systems enhanced by stacked intelligent metasurfaces (SIMs) under Rayleigh fading conditions. The proposed expression is valid for systems with a finite number of antennas and SIM elements and exhibits tightness throughout the whole signal-to-noise ratio (SNR) range. Furthermore, we conduct a comprehensive low-SNR analysis, offering meaningful observations on how key system parameters influence the capacity performance.

**Index Terms**—Holographic MIMO (HMIMO), stacked intelligent metasurfaces (SIMs), 6G networks.

## I. INTRODUCTION

Considered essential for sixth-generation (6G), reconfigurable intelligent surfaces (RIS) leverage near-passive, controllable units to reconfigure the surrounding propagation environment in real time. [1], [2]. A typical RIS comprises a number of cost-effective elements capable of inducing controllable phase shifts on incident electromagnetic waves, thereby enabling various signal enhancement objectives to support improved wireless connectivity [1].

Despite the broad applicability of RIS across diverse communication scenarios due to several inherent advantages, the majority of prior research has primarily focused on single-layer metasurface designs, which inherently limit beam management capabilities [3]. Additionally, conventional single-layer RIS designs, constrained by hardware limitations, are generally inadequate for effectively mitigating inter-user interference.

These constraints spurred the development of the stacked intelligent metasurface (SIM) paradigm by An *et al.* [4], which offers notable improvements over traditional single-layer RIS. Specifically, a SIM-assisted transceiver architecture was proposed for point-to-point MIMO configurations, with one SIM at the transmitter and another at the receiver, enabling electromagnetic (EM) wave propagation through the metasurfaces. Among the key advantages of SIM technology are its enhanced computational efficiency, ultrafast processing capabilities, lower computational complexity, reduced reliance on RF chains, and decreased energy consumption, which position it as a promising enabler for sixth-generation (6G) communication systems. In this context, the achievable rate performance of SIM-assisted systems in multi-user MISO configurations was examined in [5], [6] under certain conditions, while aspects of near-field

A. Papazafeiropoulos is with the Communications and Intelligent Systems Research Group, University of Hertfordshire, Hatfield AL10 9AB, U. K. Ioannis Bartsikas and Dimitra I. Kaklamani are with the Microwave and Fiber Optics Laboratory, and Iakovos S. Venieris is with the Intelligent Communications and Broadband Networks Laboratory, School of Electrical and Computer Engineering, National Technical University of Athens, Zografou, 15780 Athens, Greece. Corresponding author's email: tapapazaf@gmail.com. This work is financially supported by EPSRC/DSIT Federated Telecoms Hub - TITAN (6G-DISCO).

beamforming were explored in [7].<sup>1</sup>

In this letter, we first provide a general closed-form lower bound on the ergodic capacity of SIM-assisted MIMO system and a study of the low-SNR regime. Specifically, the proposed general lower bound applies to systems with an arbitrary number of SIM elements at both ends and maintains tightness across the full SNR regime. Compared with existing works, this paper advances the analysis of SIM-assisted HMIMO systems in several key ways. While [4] and [5] investigate achievable rates or hybrid SIM architectures, they do not provide closed-form ergodic capacity expressions. Also, classical bounds such as [14] address correlated MIMO channels but do not model the metasurface-induced transformations introduced by SIMs. Furthermore, the proposed projected-gradient framework enables joint optimization of all SIM phase profiles, which is not available in [4] or [14]. Moreover, a detailed second-order analysis in the low-SNR region is conducted, yielding closed-form expressions for key performance metrics, which are the minimum energy per bit (EB) and the wideband slope (WS) that characterize MIMO system behavior in this regime.

## II. SYSTEM MODEL

We focus on a point-to-point SIM-aided HMIMO model with SIM integration at both transmission and reception ends. Each SIM interfaces with an intelligent controller responsible for tuning the phase of the electromagnetic wave impinging on each meta-atom of every surface. The transmitter is equipped with  $N_t$  antennas, while the receiver is configured with  $N_r$  antennas. According to the SIM architecture in [4], [10], let  $L$  and  $M$  be the total number of layers and the corresponding number of meta-atoms in each layer within the transmit-side SIM. Moreover, let  $K$  and  $N$  be the number of layers and the per-layer meta-atom count at the receiver SIM. Also, we define  $s \triangleq \min(M, N)$  and  $t \triangleq \max(M, N)$ .

### A. Layer-Wise Phase Control for Stacked Metasurfaces

Let  $\mathcal{L}$  and  $\mathcal{K}$  denote the index sets of the transmit- and receive-side layers, respectively. Each transmit layer comprises  $M$  meta-atoms indexed by  $\mathcal{M} = \{1, \dots, M\}$ , while each receive layer comprises  $N$  elements indexed by  $\mathcal{N} = \{1, \dots, N\}$  as mentioned. We adopt unit-modulus phase control at every element. For the  $l$ -th transmit layer ( $l \in \mathcal{L}$ ), define the per-element phase angles  $\theta_m^l \in [0, 2\pi)$ ,  $m \in \mathcal{M}$ , and the corresponding complex weights  $\phi_m^l \triangleq e^{j\theta_m^l}$ , which are stacked into the vector and diagonal transmission matrix

$$\boldsymbol{\phi}^l \triangleq [\phi_1^l, \dots, \phi_M^l]^\top \in \mathbb{C}^{M \times 1}, \quad \boldsymbol{\Phi}^l \triangleq \text{diag}(\boldsymbol{\phi}^l) \in \mathbb{C}^{M \times M}. \quad (1)$$

<sup>1</sup>It is also important to acknowledge that practical metasurface implementations exhibit non-idealities such as phase–amplitude coupling and tuning inaccuracies. Recent works on stacked and holographic metasurfaces [8], [9] have shown that impairments can affect the achievable rate, indicating that hardware-aware SIM modeling is an important direction for future research.

Here,  $\Phi^l$  captures the element-wise, unit-modulus transmission coefficients applied by the  $l$ -th layer. Analogously, for the  $k$ -th receive layer ( $k \in \mathcal{K}$ ), let the per-element phase angles be  $\vartheta_n^k \in [0, 2\pi)$ ,  $n \in \mathcal{N}$ , with associated complex coefficients  $\xi_n^k \triangleq e^{j\vartheta_n^k}$ , assembled as

$$\boldsymbol{\xi}^k \triangleq [\xi_1^k, \dots, \xi_N^k]^\top \in \mathbb{C}^{N \times 1}, \quad \boldsymbol{\Xi}^k \triangleq \text{diag}(\boldsymbol{\xi}^k) \in \mathbb{C}^{N \times N}. \quad (2)$$

The diagonal matrix  $\boldsymbol{\Xi}^k$  therefore captures the receive-layer's unit-modulus, element-wise phase profile.

Overall, the transmitter and receiver SIMs are expressed as

$$\mathbf{P} = \Phi^L \mathbf{W}^L \dots \Phi^2 \mathbf{W}^2 \Phi^1 \mathbf{W}^1 \in \mathbb{C}^{M \times N_t}, \quad (3)$$

$$\mathbf{D} = \mathbf{U}^1 \boldsymbol{\Xi}^1 \mathbf{U}^2 \boldsymbol{\Xi}^2 \dots \mathbf{U}^K \boldsymbol{\Xi}^K \in \mathbb{C}^{N_r \times N}. \quad (4)$$

For  $l \in \mathcal{L} \setminus \{1\}$ , let  $\mathbf{W}^l \in \mathbb{C}^{M \times M}$  denote the transmission-coupling matrix that characterizes the interaction between the  $(l-1)$ -th and  $l$ -th transmit layers. Similarly, for  $k \in \mathcal{K} \setminus \{1\}$ , let  $\mathbf{U}^k \in \mathbb{C}^{N \times N}$  represent the transmission-coupling matrix describing the interaction between the  $(k-1)$ -th and  $k$ -th receive layers. The external interfaces are modeled as follows.  $\mathbf{W}^1 \in \mathbb{C}^{M \times N_t}$  maps the  $N_t$  transmit RF chains (or feed ports) to the first transmit SIM layer, whereas  $\mathbf{U}^1 \in \mathbb{C}^{N_r \times N}$  maps the final receive SIM layer to the  $N_r$ -element receive antenna array. The transmission coefficients at both the transmitter and the receiver can be written based on the Rayleigh-Sommerfeld diffraction theory [4].

The overall  $\mathbf{H} \in \mathbb{C}^{N_r \times N_t}$  channel can be expressed as  $\mathbf{H} = \mathbf{D}\mathbf{G}\mathbf{P}$ , where  $\mathbf{G} = \mathbf{R}_R^{1/2} \tilde{\mathbf{G}} \mathbf{R}_T^{1/2}$  is the  $N \times M$  HMIMO channel matrix linking the transmit and receive SIM layers [11]. Herein,  $\mathbf{R}_R \in \mathbb{C}^{N \times N}$  and  $\mathbf{R}_T \in \mathbb{C}^{M \times M}$  are the spatial correlation matrices associated with the receive- and transmit-side SIMs, respectively. The mathematical expressions of these spatial correlation matrices are given by [12]. In addition,  $\tilde{\mathbf{G}} \sim \mathcal{CN}(\mathbf{0}, \frac{\beta}{M} \mathbf{I}_N \otimes \mathbf{I}_M) \in \mathbb{C}^{N \times M}$  is the independent Rayleigh fading channel with  $\beta$  denoting the average path loss between the two SIMs, which is given by [13].<sup>2</sup>

The receiver obtains  $\mathbf{y} \in \mathbb{C}^{N_r}$ , which is given by

$$\mathbf{y} = \mathbf{H}\mathbf{s} + \mathbf{n} \quad (5)$$

with  $\mathbf{s} \in \mathbb{C}^{N_t}$  being the transmitted signal, where  $\mathbb{E}\{|s_i|^2\} = \frac{P}{N_t}$ ,  $i = 1, \dots, N_t$  with  $P$  expressing the total transmit power. Also,  $\mathbf{n} \in \mathbb{C}^{N_r} \sim \mathcal{CN}(\mathbf{0}, \sigma^2 \mathbf{I}_{N_r})$  represents the additive white Gaussian noise (AWGN) with variance  $\sigma^2$ .

### III. LOWER BOUND ON THE ERGODIC CAPACITY

By assuming perfect CSI at the receiver and no CSI at the transmitter, uniform power allocation across all data streams is a sensible choice. In this case, the SIM-aided HMIMO ergodic capacity in bits/s/Hz is expressed as

$$C_{\text{erg}} = \mathbb{E} \left[ \log_2 \left( \det \left( \mathbf{I}_{N_t} + \frac{\rho}{N_t} \mathbf{H}^\text{H} \mathbf{H} \right) \right) \right], \quad (6)$$

where  $\rho = \frac{P}{\sigma^2}$  is the signal-to-noise ratio (SNR).

<sup>2</sup>Although  $\mathbf{G}$  follows a Kronecker correlation model, the composite channel  $\mathbf{H} = \mathbf{D}\mathbf{G}\mathbf{P}$  becomes highly non-trivial due to SIM-induced multilayer coupling and correlation. The derived lower bound incorporates these effects through  $\mathbf{P}$ ,  $\mathbf{D}$ , and the correlation matrices, extending classical Wishart-based capacity results to the stacked SIM architecture, which provides the first tractable analytical characterization for such systems.

*Theorem 1:* The ergodic capacity of a SIM-aided HMIMO system admits a lower bound given by

$$C_{\text{erg}} \geq C_{\text{LB}} = N_t \log_2 \left( 1 + \frac{\rho}{N_t} \exp \left( \frac{1}{N_t} \left( \sum_{i=0}^{s-1} \psi(t-i) \right. \right. \right. \right. \\ \left. \left. \left. \left. + \ln |\mathbf{P}\mathbf{P}^\text{H}| + \ln |\mathbf{D}^\text{H}\mathbf{D}| + \ln |\mathbf{R}_T| + |\mathbf{R}_R| \right) \right) \right) \quad (7)$$

with  $\psi(x)$  being the digamma function [13, eq. (8.360.1)].

*Proof:* Please see Appendix A. ■

*Remark 1:* We observe that  $C_{\text{LB}}$  simplifies to the lower bound obtained in [14, Eq. 5].

The optimization problem is mathematically described as

$$(\mathcal{P}) \quad \max_{\phi_l, \xi_k} C_{\text{LB}} = f(\phi_l, \xi_k), \quad (8a)$$

$$\mathbf{P} = \Phi^L \mathbf{W}^L \dots \Phi^2 \mathbf{W}^2 \Phi^1 \mathbf{W}^1, \quad (8b)$$

$$\mathbf{Z} = \mathbf{U}^1 \boldsymbol{\Xi}^1 \mathbf{U}^2 \boldsymbol{\Xi}^2 \dots \mathbf{U}^K \boldsymbol{\Xi}^K, \quad (8c)$$

$$\boldsymbol{\Phi}^l = \text{diag}(\phi_1^l, \dots, \phi_M^l) \quad \boldsymbol{\Xi}^k = \text{diag}(\xi_1^k, \dots, \xi_N^k), \quad (8d)$$

$$|\phi_m^l| = 1, |\xi_n^k| = 1. \quad (8e)$$

It is evident that the optimization problem  $(\mathcal{P})$  is classified as nonconvex, since the objective function does not exhibit concavity or convexity with respect to the optimization variables and is further constrained by non-convex constant modulus conditions. Prior work on SIM-assisted systems has predominantly utilized alternating optimization (AO), where the transmit and receive SIM phase shifts are updated alternately. Although AO is relatively straightforward to implement, its convergence often requires numerous iterations, particularly as the size of the SIM configuration increases [15]. In the context of SIM-assisted HMIMO architectures, where every individual metasurface typically comprises a substantial number of elements, AO becomes computationally inefficient. These considerations encourage the adoption of a more effective approach based on the projected gradient method, inspired by techniques in [15], which enables concurrent optimization of the phase shifts at both the transmitter- and receiver-side SIMs.

To address the optimization problem in (8), we introduce the proposed algorithm in Algorithm 1. The core principle involves initializing from a feasible point  $(\phi_l^0, \xi_k^0)$  and iteratively updating the variables along the gradient direction  $\nabla f(\phi_l, \xi_k)$ . The step size for each update is governed by the positive parameters  $\mu_n^q > 0$ , for  $q = 1, 2$ .

The algorithm operates within the subsequent feasible sets

$$\Phi_l = \{\phi_l \in \mathbb{C}^{M \times 1} : |\phi_l^i| = 1, ; i = 1, \dots, M\}, \quad (9)$$

$$\Xi_k = \{\xi_k \in \mathbb{C}^{N \times 1} : |\xi_k^i| = 1, ; i = 1, \dots, N\}. \quad (10)$$

At each iteration, before proceeding along the gradient direction of  $f(\phi_l, \xi_k)$ , the updated variables are projected back onto their respective feasible sets  $\Phi_l$  and  $\Xi_k$ . This ensures that the iterates remain within the allowable domain of the problem. For completeness, we also provide the gradient components  $\nabla_{\phi_l} f(\phi_l, \xi_k)$  and  $\nabla_{\xi_k} f(\phi_l, \xi_k)$ , which represent the directions of the steepest ascent for the objective function  $f$ , as defined in [16, Theorem 3.4]. The operators  $P_{\Phi_l}(\cdot)$  and  $P_{\Xi_k}(\cdot)$  correspond to projections onto  $\Phi_l$  and  $\Xi_k$ , respectively.

*Lemma 1:* The complex derivatives of  $f(\phi_l, \xi_k)$  regarding the conjugate variables  $\phi_l^*$  and  $\xi_k^*$  are computed as

$$\nabla_{\phi_l} f(\phi_l, \xi_k) = \bar{V} \text{diag}(\mathbf{A}_l (\mathbf{P}^\text{H} \mathbf{P})^{-1}), \quad (11)$$

$$\nabla_{\xi_k} f(\phi_l, \xi_k) = \bar{V} \text{diag}(\mathbf{C}_k (\mathbf{D} \mathbf{D}^\text{H})^{-1}), \quad (12)$$

**Algorithm 1** Projected Gradient Ascent Method

---

```

1: Input:  $\phi_l^0, \xi_k^0, \mu_i^q > 0$  for  $q = 1, 2$ .
2: for  $i = 1, 2, \dots$  do
3:    $\phi_l^{i+1} = P_{\Phi_l}(\phi_l^i + \mu_i^1 \nabla_{\phi_l} f(\phi_l^i, \xi_k^i))$ 
4:    $\xi_k^{i+1} = P_{\Xi_k}(\xi_k^i + \mu_i^2 \nabla_{\xi_k} f(\phi_l^i, \xi_k^i))$ 
5: end for

```

---

$$\text{where } \bar{V} = \frac{\rho V}{\ln 2N_t \left(1 + \frac{\rho}{N_t} V\right)},$$

$$\mathbf{A}_l = \mathbf{W}^l \Phi^{l-1} \mathbf{W}^{l-1} \dots \Phi^1 \mathbf{W}^1 \Phi^L \mathbf{W}^L \dots \Phi^{l+1} \mathbf{W}^{l+1}, \quad (13)$$

$$\mathbf{C}_k = \mathbf{U}^l \Xi^{l-1} \mathbf{U}^{l-1} \dots \Xi^1 \mathbf{U}^1 \Xi^L \mathbf{U}^L \dots \Xi^{l+1} \mathbf{U}^{l+1}. \quad (14)$$

*Proof:* Please see Appendix B.  $\blacksquare$

The optimization framework of the SIM leverages the gradient ascent method, offering a notable benefit due to the availability of a closed-form expression for the gradient. Since the updates constitute projected gradient ascent over compact unit-modulus sets and  $C_{LB}$  is smooth and bounded, standard results guarantee convergence to a stationary point for suitable step sizes [4], [5]. The convergence curve in the numerical section further confirms rapid monotonic convergence in practice.

The computational complexity of Algorithm 1 is mainly determined by the evaluation of the lower-bound expression and its gradients in (7), (11), and (12). Each iteration requires computing the composite SIM matrices on the transmit and receive sides, which incurs a cost of  $\mathcal{O}(LM^2N_t + KN^2N_r)$ . The subsequent formation and inversion of the covariance-related matrices, as well as the determinant and gradient calculations, contribute an additional  $\mathcal{O}(M^3 + N^3 + N_t^3 + N_r^3)$ . Therefore, the overall per-iteration complexity is  $\mathcal{O}(LM^2N_t + KN^2N_r + M^3 + N^3 + N_t^3 + N_r^3)$ , which corresponds to the cost of computing all terms required by the gradient-based updates in Algorithm 1. More specifically, this cost scales linearly with the number of SIM layers, while scaling cubic in the meta-atom and antenna dimensions.

#### IV. LOW-SNR REGIME

According to [17], the operation of MIMO systems in the low-SNR region is better captured by the normalized transmit EB  $E_b/N_0$  as opposed to the conventional per-symbol SNR metric. This leads to the following capacity formulation  $C_{erg} \left( \frac{E_b}{N_0} \right) \approx S_0 \log_2 \left( \frac{\frac{E_b}{N_0}}{\frac{E_b}{N_{0\min}}} \right)$ , where  $\frac{E_b}{N_{0\min}}$  denotes the minimum normalized EB necessary to support any positive transmission rate reliably, while  $S_0$  represents the WS, both serving as key indicators of low-SNR performance. Based on [18], these two key performance metrics are defined as  $\frac{E_b}{N_{0\min}} = \frac{1}{\dot{C}_{erg}(0)}$ ,  $S_0 = -2 \ln 2 \frac{(\dot{C}_{erg}(0))^2}{\ddot{C}_{erg}(0)}$ , where  $\dot{C}_{erg}(0)$  and  $\ddot{C}_{erg}(0)$  represent the first- and second-order derivatives of the ergodic capacity in (6) with respect to the SNR  $\rho$ , respectively. As outlined in [17], analyzing the low-SNR regime involves utilizing the concept of the dispersion of a random matrix.

*Definition 1:* The dispersion of an  $s \times s$  random matrix is defined as follows  $\zeta(\mathbf{A}) = s \frac{\mathbb{E}[\text{tr}(\mathbf{A}^2)]}{\text{tr}(\mathbf{A})}$ .

*Theorem 2:* In a SIM-assisted HMIMO system with dimensions  $N_r \times N_t$ , the minimum EB and the WS are given by

$$\frac{E_b}{N_{0\min}} = N_t \ln 2 (\text{tr}(\mathbf{R}_T \mathbf{P} \mathbf{P}^H) \text{tr}(\mathbf{R}_R \mathbf{D}^H \mathbf{D}))^{-1}, \quad (15)$$

$$S_0 = \frac{2N_t N_r}{N_t \zeta(\mathbf{R}_T \mathbf{P} \mathbf{P}^H) + N_r \zeta(\mathbf{R}_R \mathbf{D}^H \mathbf{D})}. \quad (16)$$

*Proof:* Please see Appendix C.  $\blacksquare$

It is worth highlighting that, in SIM-assisted HMIMO systems, the minimum EB is influenced by the spatial correlation, whereas in conventional MIMO systems, it remains unaffected by such correlation. Furthermore, increasing the number of transmit antennas  $N_t$  generally leads to a higher minimum EB. Notably, both expressions depend on the SIMs in terms of the matrices  $\mathbf{P}$  and  $\mathbf{D}$ . Lastly, under the assumptions of i.i.d. Rayleigh fading and no SIMs, expressions (15) and (16) reduce to the results presented in [17, eq. (17)] and [17, eq. (19)], respectively.

Similar to the optimization problem  $(\mathcal{P})$ , two problems can be formulated with the same constraints, one for the minimum EB and one for the WS. The procedure is omitted since it is the same as the methodology followed in Section III.

The corresponding gradients are obtained as

$$\nabla_{\phi_l} \frac{E_b}{N_{0\min}} = -N_t \ln 2 \frac{\text{diag}(\mathbf{A}_l \mathbf{R}_T \mathbf{P}^H \mathbf{P})}{(\text{tr}(\mathbf{R}_T \mathbf{P} \mathbf{P}^H) \text{tr}(\mathbf{R}_R \mathbf{D}^H \mathbf{D}))^2}, \quad (17)$$

$$\nabla_{\xi_k} \frac{E_b}{N_{0\min}} = -N_t \ln 2 \frac{\text{diag}(\mathbf{C}_k \mathbf{R}_R \mathbf{D} \mathbf{D}^H)}{(\text{tr}(\mathbf{R}_T \mathbf{P} \mathbf{P}^H) \text{tr}(\mathbf{R}_R \mathbf{D}^H \mathbf{D}))^2}, \quad (18)$$

$$\nabla_{\phi_l} S_0 = -\frac{2N_t^2 N_r s}{(N_t \zeta(\mathbf{R}_T \mathbf{P} \mathbf{P}^H) + N_r \zeta(\mathbf{R}_R \mathbf{D}^H \mathbf{D}))^2 \text{tr}^2(\mathbf{R}_T \mathbf{P} \mathbf{P}^H)} \quad (19)$$

$$\times \text{diag}(2 \text{tr}(\mathbf{R}_T \mathbf{P} \mathbf{P}^H) \mathbf{A}_l \mathbf{P}^H \mathbf{P} \mathbf{R}_T \mathbf{P}^H \mathbf{R}_T \quad (20)$$

$$- \text{tr}((\mathbf{R}_T \mathbf{P} \mathbf{P}^H)^2 \mathbf{A}_l \mathbf{R}_T)), \quad (21)$$

$$\nabla_{\xi_k} S_0 = -\frac{2N_t^2 N_r s}{(N_t \zeta(\mathbf{R}_T \mathbf{P} \mathbf{P}^H) + N_r \zeta(\mathbf{R}_R \mathbf{D}^H \mathbf{D}))^2 \text{tr}^2(\mathbf{R}_R \mathbf{D}^H \mathbf{D})} \quad (22)$$

$$\times \text{diag}(2 \text{tr}(\mathbf{R}_R \mathbf{D}^H \mathbf{D}) \mathbf{C}_k \mathbf{D} \mathbf{D}^H \mathbf{R}_R \mathbf{D} \mathbf{R}_R \quad (23)$$

$$- \text{tr}((\mathbf{R}_R \mathbf{D}^H \mathbf{D})^2 \mathbf{C}_k \mathbf{R}_R)). \quad (24)$$

*Proof:* The proof is omitted due to limited space and because it follows the steps of the proof of Lemma 1 since the dependence of  $\frac{E_b}{N_{0\min}}$  and  $S_0$  from  $\mathbf{P}$  and  $\mathbf{D}$  is similar to the dependence of  $C_{LB}$  from these parameters.  $\blacksquare$

The complexity of the two algorithms is similar to problem  $(\mathcal{P})$  since their implementation involves similar matrix operations.

#### V. NUMERICAL RESULTS

The analytical expressions and Monte Carlo (MC) simulation results are used for validation. In the simulated setup, the SIMs at the transmitter and receiver are placed along the  $x$ - $z$  plane, with their centers being along the  $y$ -axis at an altitude of  $H_{BS} = 5$  m. The design and configuration of both SIMs adhere to the methodology outlined in [4], [10]. Each meta-atom occupies an area of  $(\lambda/2)^2$ , and the distance separating neighboring meta-atoms is fixed at  $\lambda/2$ . The gap between the two metasurfaces is given by  $d_{\text{SIM}} = T_{\text{SIM}}/L$ , where  $T_{\text{SIM}} = R_{\text{SIM}} = 5\lambda$  denotes the SIM thickness. A path-loss exponent of  $b = 2.5$  is adopted. The separation

between the transmitter- and receiver-side SIMs is fixed at  $d = 200$  m. The system employs a bandwidth of 20 MHz at a carrier frequency of 2 GHz. The total transmit power is set to  $\rho = 20$  dBm, and the receiver noise (sensitivity) level is taken as  $\sigma^2 = -110$  dBm. By default, the antenna arrays comprise  $N_t = N_r = 8$  elements, each SIM contains  $M = 40$ ,  $N = 100$  meta-atoms, and the number of SIM layers is  $K = L = 4$  [4, 10].

In Fig. 1, we observe an excellent match between the analytical lower bound and Monte Carlo simulations for various  $(M, N)$  configurations, confirming the tightness of the bound across the SNR range. As expected, increasing the number of SIM meta-atoms improves the ergodic capacity. However, the figure reveals an important asymmetry: enlarging  $s = \min(M, N)$  yields a much stronger capacity gain than enlarging  $t = \max(M, N)$ , which is fully consistent with the analytical expression. The figure further includes the i.i.d. channel case and the scenario with unoptimized (random) SIM phase shifts, both showing lower performance and underscoring the impact of phase optimization on the overall SIM-assisted HMIMO gain.

Fig. 2 shows the simulated and analytical low-SNR capacity versus the transmit EB  $E_b/N_0$  according to Theorem 2. For comparative purposes, we have depicted the scenario of a conventional i.i.d. Rayleigh MIMO channel. Fig. 2 highlights a notable trade-off: although SIMs improve the ergodic capacity at moderate and high SNRs, they increase the minimum energy per bit  $E_b/N_0^{\min}$ . From Theorem 2, this metric scales with  $(\text{tr}(\mathbf{R}_T \mathbf{P} \mathbf{P}^H) \text{tr}(\mathbf{R}_R \mathbf{D} \mathbf{D}^H))^{-1}$ , which becomes larger when the SIM induces stronger spatial correlation. At very low SNR, this correlation dominates the channel behavior and reduces the effective rank, requiring more energy to reliably transmit even vanishingly small rates. This also explains the slight reduction in the wideband slope  $S_0$  in Fig. 2. In summary, SIMs enhance capacity when power is sufficient, but in the energy-limited regime their correlation-enhancing effect leads to higher required  $E_b/N_0^{\min}$ .

Fig. 3 illustrates the convergence of the projected gradient ascent scheme. In particular,  $C_{LB}$  increases monotonically and stabilizes within few iterations for different initializations. The algorithm finishes when the iterations are greater than 20 or the difference between the two last iterations is less than  $10^{-5}$ . A small-scale comparison with exhaustive search further indicates that any performance loss due to the projection step is negligible in practice.

**Discussion on the Impact of SIM Parameters:** The trends observed in Fig. 1 and Fig. 2 illustrate the impact of the SIM aperture dimensions  $(M, N)$ . Increasing the number of meta-atoms per layer enlarges the effective SIM aperture and enables finer sampling of the impinging wavefield, which enhances the spatial degrees of freedom captured by the composite matrices  $\mathbf{P}$  and  $\mathbf{D}$ . This leads to a more favorable eigenvalue distribution of  $\mathbf{G}^H \mathbf{G}$  and results in the monotonic capacity gains visible in Fig. 1. The figure also shows that changes in  $s = \min(M, N)$  have a more pronounced effect than changes in  $t = \max(M, N)$ , which means that the smallest SIM play a key role in the performance. Furthermore, increasing the number of layers  $L$  and  $K$  (not shown due to limited space) introduces additional cascaded diffraction, which enriches the spatial degrees of freedom embedded in the composite matrices  $\mathbf{P}$  and  $\mathbf{D}$ , i.e., the capacity becomes larger. These effects extend to the low-SNR regime in Fig. 2. The metrics  $E_b/N_0^{\min}$  and

$S_0$  depend on  $\text{tr}(\mathbf{R}_T \mathbf{P} \mathbf{P}^H)$  and  $\text{tr}(\mathbf{R}_R \mathbf{D} \mathbf{D}^H)$ , both of which increase with the SIM aperture size.

## VI. CONCLUSION

This letter presented a lower bound formulation for the ergodic capacity of SIM-assisted HMIMO systems. The resulting expression is mathematically tractable, valid for a finite number of antennas and SIM elements, and exhibits tightness across the SNR. In addition, a second-order capacity expansion was performed in the low-SNR regime, leading to closed-form expressions for key performance indicators, namely the minimum EB and the WS, offering valuable insights into the performance of the system. Relevant extensions include accounting for hardware impairments, imperfect CSI, and practical phase quantization in SIM layers. Incorporating these constraints is essential for translating SIM-assisted HMIMO into real-world deployments.

## APPENDIX A PROOF OF THEOREM 1

Starting from (12), Minkowski's determinant inequality yields

$$\det\left(\mathbf{I}_{N_t} + \frac{\rho}{N_t} \mathbf{H} \mathbf{H}^H\right)^{1/N_t} \geq 1 + \frac{\rho}{N_t} \det(\mathbf{H} \mathbf{H}^H)^{1/N_t},$$

leading to

$$C_{\text{erg}} \geq N_t \mathbb{E}\left[\log_2\left(1 + \frac{\rho}{N_t} e^{\frac{1}{N_t} \ln \det(\mathbf{H} \mathbf{H}^H)}\right)\right].$$

Since  $f(x) = \log_2(1 + ae^x)$  is convex for  $a > 0$ , Jensen's inequality gives

$$C_{\text{erg}} \geq N_t \log_2\left(1 + \frac{\rho}{N_t} e^{\frac{1}{N_t} \mathbb{E}[\ln \det(\mathbf{H} \mathbf{H}^H)]}\right).$$

Using  $\mathbf{H} = \mathbf{D} \mathbf{G} \mathbf{P}$  and  $\det(\mathbf{AB}) = \det(\mathbf{A})\det(\mathbf{B})$ , we have

$$\begin{aligned} \ln \det(\mathbf{H} \mathbf{H}^H) &= \ln \det(\mathbf{G}^H \mathbf{G}) + \ln |\mathbf{P} \mathbf{P}^H| \\ &\quad + \ln |\mathbf{D}^H \mathbf{D}| + \ln |\mathbf{R}_T| + \ln |\mathbf{R}_R|. \end{aligned} \quad (25)$$

For the Kronecker MIMO model,  $\mathbf{G} \in \mathbb{C}^{N \times M}$  yields a Gram matrix with  $\text{rank}(\mathbf{G}^H \mathbf{G}) = \min(M, N)$ . Using the standard Wishart result [19, A.8.1], we obtain

$$\mathbb{E}[\ln \det(\mathbf{G}^H \mathbf{G})] = \sum_{i=0}^{\min(M, N)-1} \psi(\max(M, N) - i),$$

which, when substituted into (25), yields Theorem 1.

## APPENDIX B PROOF OF LEMMA 1

The step-by-step computation of  $\nabla_{\phi_l} f(\phi_l, \xi_k)$  starts with computing its differential, given by

$$d(f(\phi_l, \xi_k)) = \frac{\rho V d(|\mathbf{P} \mathbf{P}^H|)}{\ln 2N_t \left(1 + \frac{\rho}{N_t} V\right)} \quad (26)$$

$$= \frac{\rho V \text{tr}((\mathbf{P} \mathbf{P}^H)^{-1} (d(\mathbf{P}) \mathbf{P}^H + \mathbf{P} d(\mathbf{P}^H)))}{\ln 2N_t \left(1 + \frac{\rho}{N_t} V\right)}, \quad (27)$$

where  $V = \exp\left(\frac{1}{N_t} (\sum_{i=0}^{s-1} \psi(t-i) + \ln |\mathbf{P} \mathbf{P}^H| + \ln |\mathbf{D}^H \mathbf{D}| + \ln |\mathbf{R}_T| + \ln |\mathbf{R}_R|)\right)$ . In (27), we have made use of the property

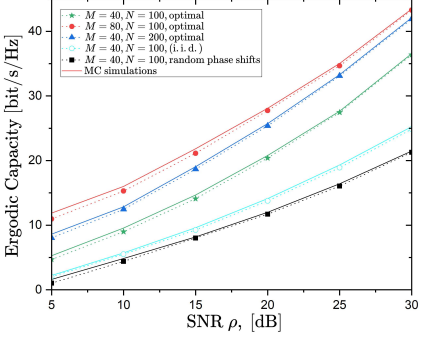


Fig. 1: Analytical lower bound and simulated ergodic capacity versus the SNR.

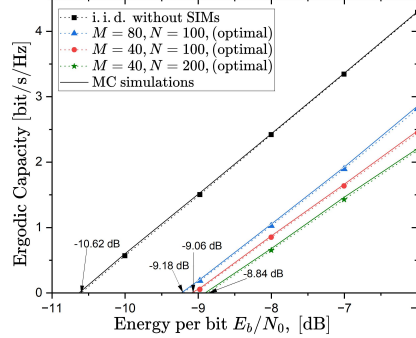


Fig. 2: Simulated and analytical low-SNR ergodic capacity versus the transmit EB.

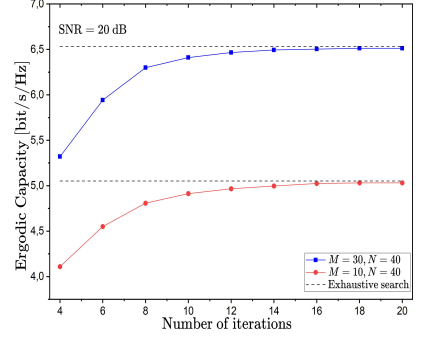


Fig. 3: Analytical lower bound with respect to the number of iterations.

$$d(|\mathbf{X}|) = |\mathbf{X}| \operatorname{tr}(\mathbf{X}^{-1} d\mathbf{X}) \text{ for a square, invertible matrix } \mathbf{X} \in \mathbb{C}^{n \times n}.$$

Additionally, the expression in (3) admits the following differential form

$$\begin{aligned} d(\mathbf{P}) &= \Phi^L \mathbf{W}^L \cdots \Phi^{l+1} \mathbf{W}^{l+1} d(\Phi^l) \mathbf{W}^l \Phi^{l-1} \\ &\quad \times \mathbf{W}^{l-1} \cdots \Phi^1 \mathbf{W}^1. \end{aligned} \quad (28)$$

Upon replacing  $d(\mathbf{P})$  with its expression in (27), we derive

$$\begin{aligned} d(f(\phi_l, \xi_k)) &= \frac{\rho V \operatorname{tr}((\mathbf{P} \mathbf{P}^H)^{-1} (\mathbf{A}_l d(\Phi^l) + \mathbf{A}_l^H d((\Phi^l)^H)))}{\ln 2 N_t \left(1 + \frac{\rho}{N_t} V\right)}, \end{aligned} \quad (29)$$

where

$$\mathbf{A}_l = \mathbf{W}^l \Phi^{l-1} \mathbf{W}^{l-1} \cdots \Phi^1 \mathbf{W}^1 \Phi^l \mathbf{W}^l \cdots \Phi^{l+1} \mathbf{W}^{l+1}. \quad (30)$$

The gradient is obtained as

$$\nabla_{\phi_l} f(\phi_l, \xi_k) = \frac{\rho V \operatorname{diag}(\mathbf{A}_l (\mathbf{P}^H \mathbf{P})^{-1})}{\ln 2 N_t \left(1 + \frac{\rho}{N_t} V\right)}. \quad (31)$$

In a similar way,  $\nabla_{\xi_k} f(\phi_l, \xi_k)$  is obtained.

## APPENDIX C PROOF OF THEOREM 2

The derivation commences by recognizing that  $\frac{d}{dx} \ln(\det(\mathbf{I} + x\mathbf{A})) \Big|_{x=0} = \operatorname{tr}(\mathbf{A})$ , which leads to the need to compute  $\mathbb{E}[\operatorname{tr}(\mathbf{H}^H \mathbf{H})]$ . Nonetheless, performing this computation directly can be quite cumbersome. To address this challenge, we employ tools from random matrix theory, drawing upon the methodology presented in [17]. Specifically, by simultaneously considering the impact of spatial correlations and passive beamforming matrices, the framework outlined in [17, Appendix B] becomes applicable. Under these conditions, the prerequisites of [17, Lemma 3] are satisfied, allowing the expression to be simplified as follows

$$\mathbb{E}[\operatorname{tr}(\mathbf{H}^H \mathbf{H})] = \operatorname{tr}(\mathbf{R}_T \mathbf{P} \mathbf{P}^H) \operatorname{tr}(\mathbf{R}_R \mathbf{D}^H \mathbf{D}). \quad (32)$$

From the combination of (6) and (32), equation (15) follows directly. The WS can be derived using the formulation provided in [17, eq. (19)] as

$$S_0 = \frac{2N_t N_r}{N_t \zeta(\mathbf{R}_T \mathbf{P} \mathbf{P}^H) + N_r \zeta(\mathbf{R}_R \mathbf{D}^H \mathbf{D})}. \quad (33)$$

## REFERENCES

- [1] M. Di Renzo *et al.*, “Smart radio environments empowered by reconfigurable intelligent surfaces: How it works, state of research, and the road ahead,” *IEEE J. Sel. Areas Commun.*, vol. 38, no. 11, pp. 2450–2525, 2020.
- [2] A. Papazafeiropoulos *et al.*, “Intelligent reflecting surface-assisted MU-MISO systems with imperfect hardware: Channel estimation and beamforming design,” *IEEE Trans. Wireless Commun.*, vol. 21, no. 3, pp. 2077–2092, 2021.
- [3] H. Guo *et al.*, “Weighted sum-rate maximization for reconfigurable intelligent surface aided wireless networks,” *IEEE Trans. Wireless Commun.*, vol. 19, no. 5, pp. 3064–3076, 2020.
- [4] J. An *et al.*, “Stacked intelligent metasurfaces for efficient holographic MIMO communications in 6G,” *IEEE J. Sel. Areas Commun.*, vol. 41, no. 8, pp. 2380–2396, 2023.
- [5] A. Papazafeiropoulos *et al.*, “Performance of double-stacked intelligent metasurface-assisted multiuser massive MIMO communications in the wave domain,” *IEEE Trans. Wireless Commun.*, vol. 24, no. 5, pp. 4205–4218, 2025.
- [6] ———, “Achievable rate optimization for large stacked intelligent metasurfaces based on statistical CSI,” *IEEE Wireless Commun. Lett.*, vol. 13, no. 9, pp. 2337–2341, 2024.
- [7] ———, “Near-field beamforming for stacked intelligent metasurfaces-assisted MIMO networks,” *accepted in IEEE Wireless Commun. Lett.*, pp. 1–1, 2024.
- [8] Q. Li *et al.*, “Stacked intelligent metasurfaces for holographic MIMO-aided cell-free networks,” *IEEE Trans. Commun.*, vol. 72, no. 11, pp. 7139–7151, 2024.
- [9] ———, “Holographic metasurface-based beamforming for multi-altitude LEO satellite networks,” *IEEE Trans. Wireless Commun.*, 2025.
- [10] A. Papazafeiropoulos *et al.*, “Achievable rate optimization for stacked intelligent metasurface-assisted holographic MIMO communications,” *IEEE Trans. Wireless Commun.*, pp. 1–1, 2024.
- [11] X. Hu *et al.*, “Holographic beamforming for ultra massive MIMO with limited radiation amplitudes: How many quantized bits do we need?” *IEEE Commun. Lett.*, vol. 26, no. 6, pp. 1403–1407, 2022.
- [12] Ö. T. Demir, E. Björnson, and L. Sanguinetti, “Channel modeling and channel estimation for holographic massive MIMO with planar arrays,” *IEEE Wireless Commun. Lett.*, vol. 11, no. 5, pp. 997–1001, 2022.
- [13] T. S. Rappaport *et al.*, “Wideband millimeter-wave propagation measurements and channel models for future wireless communication system design,” *IEEE Trans. Commun.*, vol. 63, no. 9, pp. 3029–3056, 2015.
- [14] M. Matthaiou, N. D. Chatzidiamantis, and G. K. Karagiannidis, “A new lower bound on the ergodic capacity of distributed MIMO systems,” *IEEE Signal Process. Lett.*, vol. 18, no. 4, pp. 227–230, 2011.
- [15] N. S. Perović *et al.*, “Achievable rate optimization for MIMO systems with reconfigurable intelligent surfaces,” *IEEE Trans. Wireless Commun.*, vol. 20, no. 6, pp. 3865–3882, 2021.
- [16] A. Hjørungnes, *Complex-Valued Matrix Derivatives: With Applications in Signal Processing and Communications*. Cambridge University Press, 2011.
- [17] A. Lozano, A. M. Tulino, and S. Verdú, “Multiple-antenna capacity in the low-power regime,” *IEEE Trans. Inf. Theory*, vol. 49, no. 10, pp. 2527–2544, 2003.
- [18] S. Verdú, “Spectral efficiency in the wideband regime,” *IEEE Trans. Inform. Theory*, vol. 48, no. 6, pp. 1319–1343, 2002.
- [19] A. Grant, “Rayleigh fading multi-antenna channels,” *EURASIP J. Advances Signal Process.*, vol. 2002, pp. 1–14, 2002.